

A generalized Frenet frame for computing MHD equilibria in stellarators

Florian Hindenlang¹, Gabriel G. Plunk², Omar Maj¹

¹Numerical Methods in Plasma Physics, Max Planck Institute for Plasma Physics, Garching, Germany

²Max Planck Institute for Plasma Physics, Greifswald, Germany

E-mail: florian.hindenlang@ipp.mpg.de

Abstract. For the representation of axi-symmetric plasma configurations (tokamaks), it is natural to use cylindrical coordinates (R, Z, ϕ) , where ϕ is an independent coordinate. The same cylindrical coordinates have also been widely used for representing 3D MHD equilibria of non-axisymmetric configurations (stellarators), with cross-sections, defined in (R, Z) -planes, that vary over ϕ .

Stellarator equilibria have been found, however, for which cylindrical coordinates are not at all a natural choice, for instance certain stellarators obtained using the near-axis expansion (NAE) [1, 2], defined by a magnetic axis curve and its Frenet frame.

In this contribution we demonstrate how to use an *axis-following frame* that we call a 'generalized Frenet frame', as an alternative to using cylindrical coordinates in a 3D MHD equilibrium solver. We see two advantages: 1) the capability to easily represent configurations where the magnetic axis is highly non-planar or even knotted. 2) a reduction in the degrees of freedom needed for the geometry, enabling progress in optimization of these configurations.

We discuss the definition of the generalized Frenet frame, and details of the implementation of the new frame in the 3D MHD equilibrium solver GVEC. Furthermore, we demonstrate for a highly shaped QI-optimized stellarator that far fewer degrees of freedom are necessary to find a high quality equilibrium solution, compared to the solution computed in cylindrical coordinates.

1. Introduction

In this paper, we introduce a *generalized Frenet frame*, which we denote '*G-frame*'. We claim that the *G-frame* allows us to represent the geometry of stellarators with closed 3D surfaces of basically any shape.

Similar to the conventional Frenet frame, the *G-frame* smoothly follows a curve in 3D space, with the first basis vector being the tangent unit vector to the curve and the two remaining basis vectors spanning a plane normal to the curve. An important requirement of the *G-frame* is that all its basis vectors are *defined and differentiable* everywhere along the curve parameter. This requirement is not always met by the conventional Frenet frame, as described in section 2. We mostly focus on the defining properties of the generalized Frenet frame, but provide an example of its explicit

construction. An example that naturally meets the requirements of the G -frame is the Bishop frame [3, 4], which is also called the parallel transport frame, or rotation-minimizing frame, and which can be easily constructed discretely [5]. The flexibility of the G -frame is intended to allow users to make their own definitions that suit cases of interest to them.

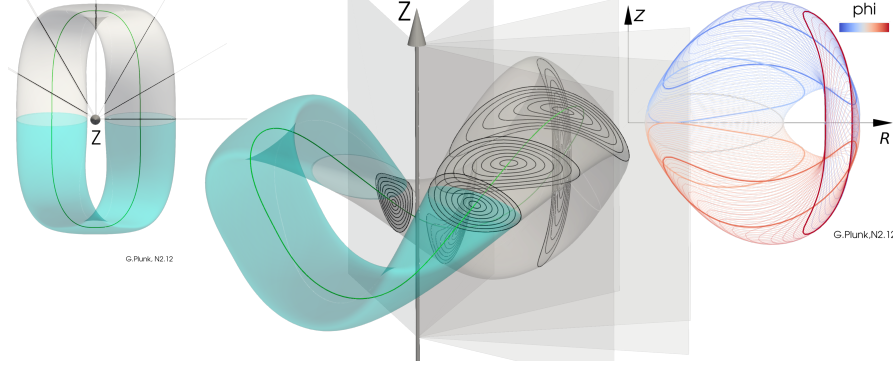
The main motivation of this work is to use the G -frame in the context of the 3D MHD equilibrium solution in stellarators. The conventional and widely used cylinder coordinates, with cross-sections in R, Z parameterized over the geometrical toroidal angle ϕ , has strong limitations on the 3D surface shapes it can represent, and thus artificially restricts the space of possible shapes that can be explored in stellarator optimization.

One of the most prominent 3D MHD equilibrium codes, founding modern computational stellarator optimization, is VMEC [6–8]. A key idea of VMEC is the assumption of closed nested flux surfaces to find 3D MHD equilibria. Note that the assumption of a continuum of nested flux surfaces does not necessarily hold in three-dimensional magnetic fields and can lead to current singularities at rational surfaces, as discussed in [9]. In VMEC, starting from an initial state of closed nested 3D surfaces, expressed in flux-aligned coordinates (or magnetic coordinates) [10], the equilibrium solution is found by minimization of the MHD energy iteratively, changing the 3D surface shapes while keeping them nested. More recently, 3D MHD equilibrium solvers following the same assumption of nested 3D surfaces have been developed, such as DESC [11] and GVEC [12], being different from each other, as well as from VMEC, in their discretization and the way the iterative solution is found.

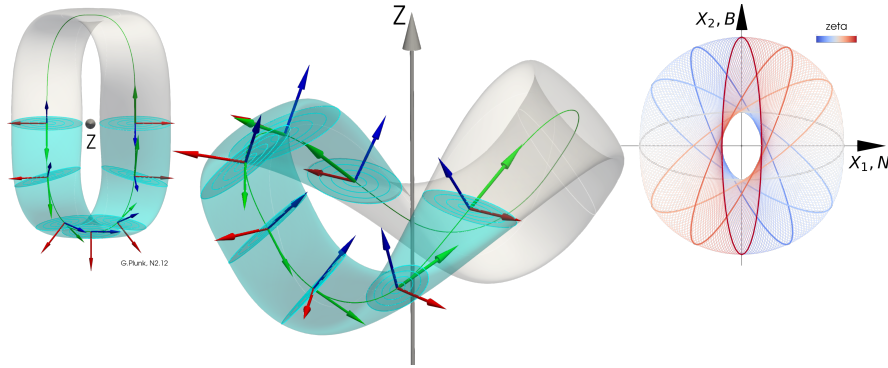
When designing GVEC, care was taken separating the actual geometry representation from its toroidal topology. In GVEC, the geometry is described by 2D cross-sections in two coordinates (q^1, q^2) and parameterized by a third periodic coordinate ζ . The mapping from (q^1, q^2, ζ) to Cartesian coordinates is not fixed and can be described by any expression. Simple examples are the periodic cylinder $(x = q^1, y = q^2, z = \zeta)$ and the conventional toroidal representation $(x = q^1 \cos(\zeta), y = q^1 \sin(\zeta), z = q^2)$. It is this feature that allows us to use the G -frame in GVEC to solve 3D MHD equilibria.

Stellarator equilibria are traditionally found by numerical optimization of their boundary shapes, to ensure that certain physical properties are satisfied, for example related to plasma confinement and stability. An alternative and elegant approach to finding optimal stellarator shapes is by use of the near axis expansion (NAE) in Boozer coordinates, as introduced by [13, 14] and extended over the last years [1, 2, 15]. Again, nested 3D flux surfaces are assumed, constrained to local MHD equilibrium conditions, and are represented as Taylor expansion around a closed parameterized 3D curve $X(\zeta)$, which is identified with the magnetic axis. Each cross-section is defined over a plane perpendicular to the axis, spanned by normal (N^F) and bi-normal (B^F) vectors of the Frenet frame of the magnetic axis. As the configurations are defined by the magnetic axis, generally an arbitrary closed curve, completely new optimized

stellarator shapes can be found for which cylindrical coordinates are not at all a natural choice. For instance, certain quasi-symmetric and quasi-isodynamic stellarators, even knotted configurations, have been obtained (or ‘constructed’) using NAE [16–18].



(a) (R, Z, ϕ) frame

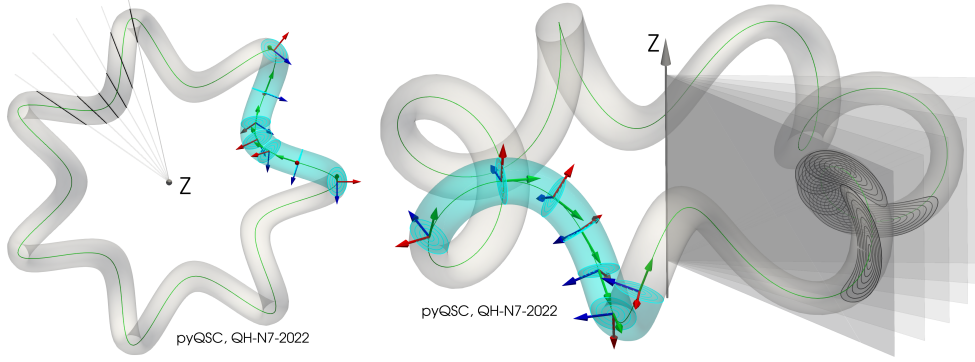


(b) Frenet frame (T green, N red, B blue)

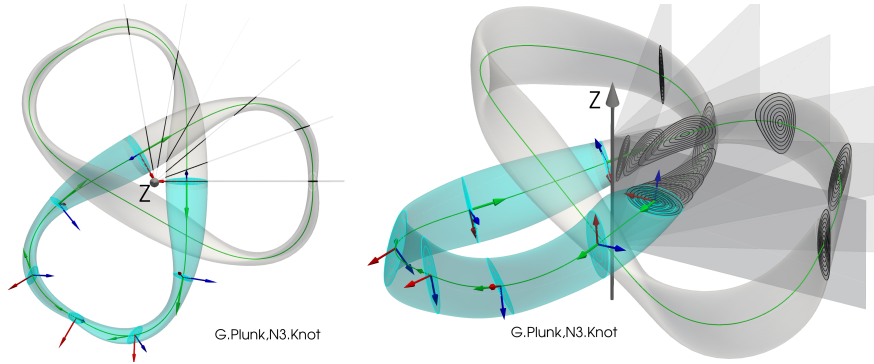
Figure 1. Comparison of (R, Z, ϕ) in and Frenet frame for a two field periodic QI-configuration N2-12 [18]. Top view (left), side view with cross-sections (middle), all cross-sections in respective frame, colored along the toroidal parametrization (right).

Using the G -frame in an MHD equilibrium solver will enable progress in optimization of new stellarator configurations. In this work we demonstrate, for the case of a highly shaped QI-optimized stellarator, that far fewer degrees of freedom are needed to find a high-quality equilibrium solution, as compared to the solution computed in cylindrical coordinates. This configuration is depicted in Fig. 1, showing highly shaped cross-sections in the (R, Z) -planes, as opposed to simple ellipses in the (N, B) -planes of the Frenet frame.

In Fig. 2, examples of a helical magnetic axis and a knotted magnetic axis are shown, where the cross-sections in the Frenet frame remain ellipses. The representation of such configurations in (R, Z) cross-sections is challenging: for the helical case the magnetic axis points in the vertical (Z) direction in some places, generating strongly elongated bean shapes, whereas for the knotted case one field period spans $\frac{2}{3}(2\pi)$ in the toroidal angle, and thus would require a range of $\phi \in [0, 4\pi)$ for the full configuration.



(a) Configuration 2022 QH nfp7 generated with pyQSC [1, 15], with 7 field periods



(b) Knotted QI-configuration from NAE [18], with 3 field periods.

Figure 2. Top view (left) and side view (right) of two configurations. The cross-sections in (R, Z) planes and in the Frenet frame are shown, one field period is colored green.

Generally, when the 'toroidal' parametrization (we will refer to ζ) is fixed as the geometric angle ϕ , it can lead to a non-optimal representation of the surface. In contrast, using a Frenet frame, the 'toroidal' parametrization is simply defined by the curve parametrization, and thus can be adapted to the surface shape that one wants to represent.

The outline of the paper is as follows: We start by introducing the conventional Frenet frame and the G -frame in section 2, then show the necessary steps to use it in the 3D MHD equilibrium solver in section 3. Finally, we show the numerical results for highly shaped stellarator in section 4.

2. The generalized Frenet frame

In order to motivate the introduction of a generalized Frenet frame (G -frame), we first introduce the conventional Frenet frame (or Frenet-Serret apparatus, or TNB-frame). It is fully defined by an arbitrary parameterized curve $X_0(\zeta)$. As we will only represent closed surfaces, the axis must be closed (periodic) and we choose $\zeta \in [0, 2\pi]$.

We will denote the tangential, normal and bi-normal vectors of the *generalized*

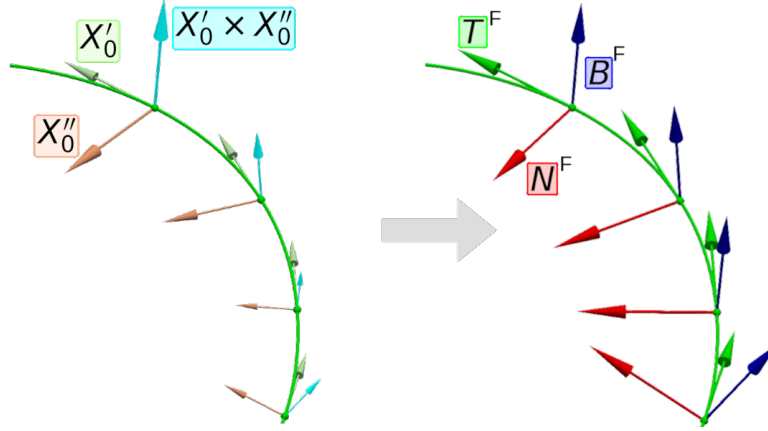


Figure 3. Construction of the local Frenet frame from first and second derivatives of the curve $X_0(\zeta)$. The curvature scales with second derivative, and thus must be $\neq 0$ to yield a valid Frenet frame.

Frenet frame by T , N , and B , respectively. To avoid confusion, we will use the superscript ' F ' when referring to the conventional Frenet frame. Note that B refers to the bi-normal and not the magnetic field. The Frenet frame satisfies the following ODE along the curve $X_0(\ell)$,

$$\frac{d}{d\ell} \begin{pmatrix} T^F \\ N^F \\ B^F \end{pmatrix} = \begin{pmatrix} \kappa(\ell)N^F \\ -\kappa(\ell)T^F + \tau(\ell)B^F \\ -\tau(\ell)N^F \end{pmatrix}, \quad (1)$$

with arc-length ℓ , curvature κ , torsion τ . The arc-length is a function of the chosen parametrization of the curve

$$\ell(\zeta) = \int_0^\zeta |X'_0(\tilde{\zeta})| d\tilde{\zeta}, \quad \ell'(\zeta) = \frac{d\ell}{d\zeta} = |X'_0(\zeta)| \quad (2)$$

As shown in Fig. 3 and (3), the Frenet frame is locally computed from the first and second derivatives of the curve

$$T^F = \frac{dX_0}{d\ell} = \frac{d\zeta}{d\ell} \frac{dX_0(\zeta)}{d\zeta} = \frac{X'_0}{|X'_0|}, \quad B^F = \frac{X'_0 \times X''_0}{|X'_0 \times X''_0|}, \quad N^F = B^F \times T^F, \quad (3)$$

and the curvature and torsion are

$$\kappa(\ell) = \frac{|X'_0 \times X''_0|}{|X'_0|^3}, \quad \tau(\ell) = \frac{(X'_0 \times X''_0) \cdot X'''_0}{|X'_0 \times X''_0|^2}. \quad (4)$$

The Frenet frame has the advantage of being defined solely by the curve. However, the following disadvantages exist:

- (i) The Frenet frame is not defined at points of zero curvature. In addition, the sign of the frame can flip when crossing such points, as shown in the top-left of Fig. 4. Zero curvature points are necessary for quasi-isodynamic stellarators [2].

- (ii) Another subtlety is that the global linking-number of the Frenet frame cannot be controlled. The linking-number is the number of rotations of the frame when following it along one turn. One would like to avoid a non-zero linking-number, for example to ensure that the rotational transform is defined in a straightforward manner. An example of a Frenet frame having a linking-number of -4 is shown top-right of Fig. 4.

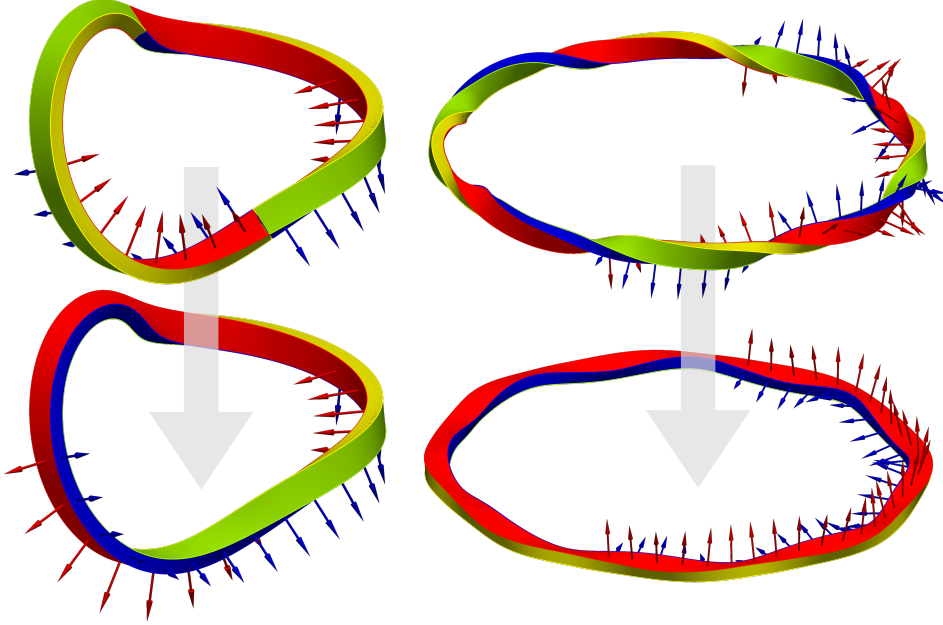


Figure 4. Visualization of the (N, B) -frame by an axis-centered rectangle swept along the axis, the surface color marks the directions $+N$ in red, $-N$ in green, $+B$ in blue and $-B$ in yellow. The Frenet frame is undefined at points of zero curvature of the axis, and the normal direction can flip sign. The sign-change shown here arises at locations of minimum field strength in quasi-isodynamic stellarators [2] (top left). The G -frame (bottom left) allows us to define a continuously differentiable frame. The Frenet frame can be twisted, here with a self-linking number of -4 (top right). The G -frame (bottom right) allows to 'untwist', yielding a self-linking number of 0.

In order to mitigate these shortcomings, we introduce the *generalized Frenet frame* (G -frame): a smooth axis-following frame that is defined by the axis position $X_0(\zeta)$, the tangential vector $X'_0(\zeta)$ as first basis vector, and the normal and bi-normal vectors $N(\zeta)$, $B(\zeta)$, which are *required to be differentiable functions* of the position along the curve. Naturally, the vectors X'_0 , N and B must form a right-handed coordinate system $X'_0 \cdot (N \times B) > 0$, but they do not need to be orthogonal. Furthermore, the generalized Frenet frame allows us to effectively undo the twist that comes about in cases of non-zero self-linking number. A visualization of the resulting G -frame is shown in the bottom of Fig. 4.

2.1. Interface to the G -frame

In GVEC, we defined an interface to the G -frame, that has the following properties:

- (i) It is assumed that $X_0(\zeta), N(\zeta), B(\zeta)$ are smoothly differentiable along the curve parameter ζ .
- (ii) The frame is given at a discrete set of points *on the full torus*

$$\zeta_i = \frac{i - 1/2}{n_p}(2\pi), \quad i = 1, \dots, n_p \quad (5)$$

- (iii) The number of points n_p must be a multiple of the field periodicity n_{FP} of the configuration, in order to be able to exactly represent a single field period.
- (iv) Cartesian coordinates are used to represent the curve position $X_0(\zeta_i)$ and normal and bi-normal vectors $N(\zeta_i), B(\zeta_i)$.

The G -frame is not unique and thus there are many ways to construct it. This flexibility in the definition of the G -frame is intended to allow users to choose a construction that suits the cases of interest to them. One prominent candidate is the Bishop frame, also called the 'parallel transport frame' [3, 4] or 'rotation-minimizing frame' [5].

Another possibility to construct a G -frame is to start from a known conventional Frenet frame, identify sign-flips and twists, then define a corresponding rotation angle function $\Gamma(\zeta)$ and apply a rigid rotation of the (N^F, B^F) plane by

$$\begin{pmatrix} T(\zeta) \\ N(\zeta) \\ B(\zeta) \end{pmatrix} = \begin{pmatrix} 1 & 0 & 0 \\ 0 & \cos(\Gamma(\zeta)) & \sin(\Gamma(\zeta)) \\ 0 & -\sin(\Gamma(\zeta)) & \cos(\Gamma(\zeta)) \end{pmatrix} \begin{pmatrix} T^F(\zeta) \\ N^F(\zeta) \\ B^F(\zeta) \end{pmatrix}. \quad (6)$$

In the present work, we compute the G -frame from the Frenet frame along the magnetic axis of a NAE configuration [18]. Since the frame was constructed solving the ODE (1) with a given *signed* curvature function and torsion, the sign-flips at zero curvature are already mitigated. Additionally, in the N2-12 case, a self-linking number (or helicity) of $(-1/2)$ within one field period was specified, which again introduces a sign-flip between field-periods. We 'untwist' the self-linking number by using equation (6), with a saw-tooth like rotation function

$$\Gamma^{\text{N2-12}}(\zeta) = -\pi \left(\frac{n_{\text{FP}}}{2\pi} \zeta - \left\lfloor \frac{n_{\text{FP}}}{2\pi} \zeta \right\rfloor \right), \quad \zeta \in [0, 2\pi], \quad (7)$$

where the jump of the rotation function is chosen to exactly cancel the sign-flip of the Frenet frame. Furthermore, due to the choice of the point positions (5), the discrete point set excludes the points of zero curvature at $\zeta = [1, 3, \dots, 2n_{\text{FP}} - 1] \frac{\pi}{n_{\text{FP}}}$ as well as the points where the rotation function jumps, at $\zeta = [0, 2, \dots, 2n_{\text{FP}}] \frac{\pi}{n_{\text{FP}}}$.

3. MHD equilibrium in the new frame

3.1. MHD equilibrium

In GVEC, we adopt essentially the same approach as in VMEC [6] to compute the MHD equilibrium. First, under the assumption of closed nested flux surfaces, the geometry is defined by an embedding map

$$f : (\rho, \vartheta, \zeta) \mapsto (x, y, z), \quad (8)$$

mapping from flux-aligned coordinates (a radial coordinate proportional to the square root of the toroidal magnetic flux, $\rho \sim \sqrt{\Phi}$ and two periodic coordinates ϑ, ζ) to Cartesian coordinates (x, y, z) . We decompose the full map $f := h \circ \tilde{X}$ with

$$\tilde{X} : (\rho, \vartheta, \zeta) \mapsto (q^1, q^2, \zeta) = (X^1(\rho, \vartheta, \zeta), X^2(\rho, \vartheta, \zeta), \zeta) \quad (9)$$

$$h : (q^1, q^2, \zeta) \mapsto (x, y, z) = h(q^1, q^2, \zeta) \quad (10)$$

leaving X^1, X^2 as functions of (ρ, ϑ, ζ) to describe the geometry of each cross-section along ζ . The map h is fixed through the equilibrium calculation but can be arbitrarily specified by the user at the beginning. Simple examples of h are given by the periodic cylinder $(x, y, z) := (q^1, q^2, \zeta)$ and the conventional toroidal representation $(x, y, z) := (q^1 \cos \zeta, q^1 \sin \zeta, q^2) = (R \cos \phi, R \sin \phi, Z)$.

The magnetic field is defined by the geometry, an additional angle transformation $\lambda(\rho, \vartheta, \zeta)$ and the rotational transform profile $\iota(\rho) = \chi'(\rho)/\Phi'(\rho)$, with the poloidal magnetic flux χ ,

$$\mathbf{B} = \frac{1}{\sqrt{g}}(b^\vartheta e_\vartheta + b^\zeta e_\zeta), \quad b^\vartheta := (\chi' - \Phi' \partial_\zeta \lambda), \quad b^\zeta := \Phi'(1 + \partial_\vartheta \lambda). \quad (11)$$

Finally, the equilibrium, defined by the flux surface geometry (X^1, X^2) and λ , is found via minimization of total MHD energy:

$$\begin{aligned} W(X^1, X^2, \lambda) &= \int_\Omega \frac{1}{2\mu_0} \mathbf{B}^2 + \frac{p(\rho)}{\gamma - 1} dV \\ &= \int_0^1 \int_0^{2\pi} \int_0^{2\pi} \left(\frac{1}{2\mu_0} \frac{1}{\sqrt{g}} (b^\vartheta g_{\vartheta\zeta} b^\zeta) + \frac{p(\rho)}{\gamma - 1} \sqrt{g} \right) d\rho d\vartheta d\zeta, \end{aligned} \quad (12)$$

with a given pressure profile $p(\rho)$ and total toroidal flux $\Phi(1)$.

As the full map f is decomposed into $f = h \circ \tilde{X}$, the metric terms in (12) are computed as

$$\sqrt{g} = \sqrt{G} \left(\frac{\partial X^1}{\partial \rho} \frac{\partial X^2}{\partial \vartheta} - \frac{\partial X^2}{\partial \rho} \frac{\partial X^1}{\partial \vartheta} \right), \quad g_{\alpha\beta} = \frac{\partial q^i}{\partial \alpha} G_{ij} \frac{\partial q^j}{\partial \beta}, \quad G_{ij} = \frac{\partial h}{\partial q^i} \cdot \frac{\partial h}{\partial q^j}, \quad (13)$$

with $(q^1, q^2, q^3) := (X^1, X^2, \zeta)$ and $i, j = 1, 2, 3$ and $\alpha, \beta \in [\rho, \vartheta, \zeta]$.

3.2. Computing the metric terms in the new frame

We will now define the map h using the G -frame from section 2.1,

$$h : (q^1, q^2, \zeta) \mapsto (x, y, z) = X_0(\zeta) + q^1 N(\zeta) + q^2 B(\zeta). \quad (14)$$

In order to compute the metric terms in (13), we need first derivatives of X_0, N, B

$$\frac{\partial h}{\partial q^1} = N, \quad \frac{\partial h}{\partial q^2} = B, \quad \frac{\partial h}{\partial q^3} = \frac{\partial h}{\partial \zeta} = X'_0 + q^1 N' + q^2 B' =: \tilde{T}_q. \quad (15)$$

Then the metric tensor and determinant of h amount to

$$G = \begin{bmatrix} |N|^2 & N \cdot B & N \cdot \tilde{T}_q \\ & |B|^2 & B \cdot \tilde{T}_q \\ \text{symm.} & & |\tilde{T}_q|^2 \end{bmatrix}, \quad \mathcal{J}_h := \sqrt{\det(G)}. \quad (16)$$

Note that this coordinates system is valid only in a limited region around the curve. The coordinates become invalid in the direction of the normal of the Frenet frame $N^F(\zeta)$ at a distance of the curvature radius $1/\kappa(\zeta)$.

When computing variations of the MHD energy with respect to X^1, X^2 , we also need to compute the derivatives of \mathcal{J}_h, G with respect to q^1, q^2 . These are found in Appendix A.

4. Application to a highly shaped stellarator

In this section, we will run GVEC with the new feature, using the G -frame for the map h . We compare the results with the GVEC solution computed with h given in cylindrical coordinates, which will be referred to as the 'RZ-frame' in the following. The data of all simulations in this section is openly available at <https://doi.org/10.5281/zenodo.13960848>.

As a challenging example, we start from the first order NAE solution of the two field periodic QI-configuration N2-12 [18], already shown in Fig. 1b. The average minor radius \bar{a} is computed from the cross-section area in the (N, B) -plane, averaged over the arc-length parameter ℓ of the axis (2), as

$$\pi \bar{a}^2 := \frac{1}{\ell(2\pi)} \int_0^{2\pi} |N \times B| \left| \frac{1}{2} \int_0^{2\pi} \left(\frac{\partial X_b^2}{\partial \vartheta} X_b^1 - \frac{\partial X_b^1}{\partial \vartheta} X_b^2 \right) d\vartheta \right| \ell'(\zeta) d\zeta, \quad (17)$$

using the boundary coordinates $X_b^1(\vartheta, \zeta), X_b^2(\vartheta, \zeta)$. The G -frame and the boundary are given by the NAE solution. For the N2-12 case, the axis length is $\ell(2\pi) = 2\pi$ meters and the average minor radius is $\bar{a} = 0.186756$ meters. The iota profile is constant and set to the on-axis value $\iota = 0.7$ and zero pressure is used, as assumed for the NAE. The average of the magnetic field strength on axis is $B_0 = 1$ Tesla.

In order to run the same case in the RZ -frame, the boundary must be transformed by finding the cross-sections on planes $\phi = \text{constant}$ of the geometric toroidal angle ϕ .

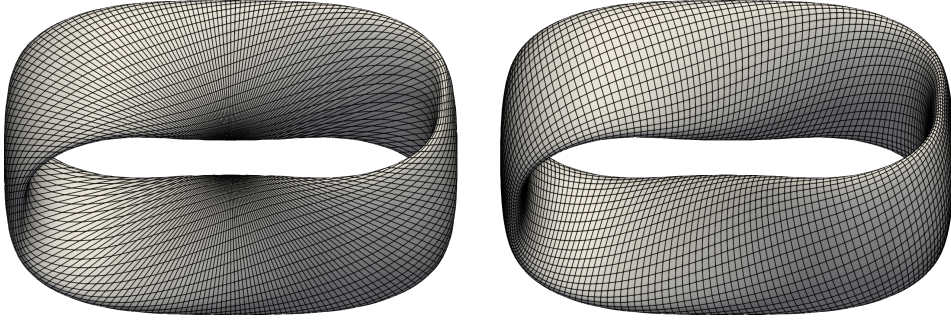


Figure 5. Top view of the boundary parametrization of the 'N2-12' configuration, left using the RZ -frame with $(m, n)_{\max} = (10, 15)$ and right the G -frame with $(m, n)_{\max} = (2, 10)$.

The change in parametrization is depicted in Fig. 5. The Fourier resolution of the boundary in the G -frame is $(m, n)_{\max} = (2, 10)$, whereas in the RZ -frame, a higher resolution of $(m, n)_{\max} = (10, 15)$ is needed to accurately represent the same boundary surface.

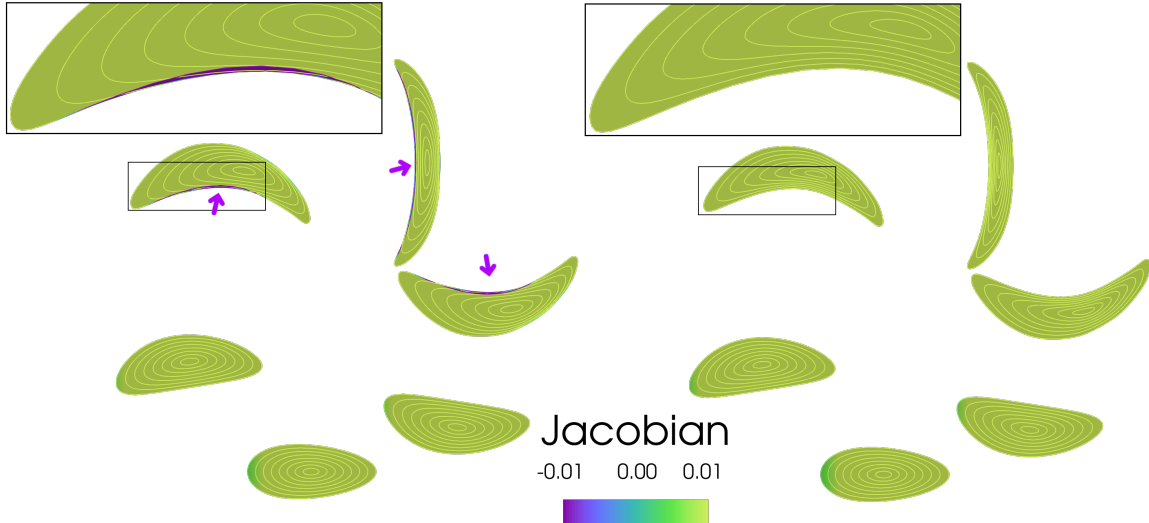


Figure 6. Cross-sections in the RZ -frame over half field period of the 'N2-12' configuration. On the left: Initial guess of the ρ contours, producing an invalid initial map with negative Jacobian close to the boundary (arrows) and a zoomed-in cross-section. On the right: the same view of the valid initial map after application of an action principle [19].

Since cross-sections in the RZ -frame are strongly shaped, the initial guess in GVEC produces a invalid map (negative Jacobian determinant), prohibiting the solver to start the minimization. The same problem occurs in VMEC. Fortunately, we were able to find a valid initial guess, using a recently proposed action principle [19] that we have implemented in GVEC, see Fig. 6.

We choose the following resolution parameters for the equilibrium runs in GVEC:

For the G -frame, we choose a radial resolution of 2 B-spline elements of degree 5 and a Fourier resolution of $(m, n)_{\max} = (2, 10)$. For the RZ -frame, we choose a radial resolution of 8 B-spline elements of degree 5 and a Fourier resolution of $(m, n)_{\max} = (10, 15)$. The minimization in GVEC converged in 800 iterations with the G -frame and in 16,000 with the RZ -frame, due to the higher resolution.

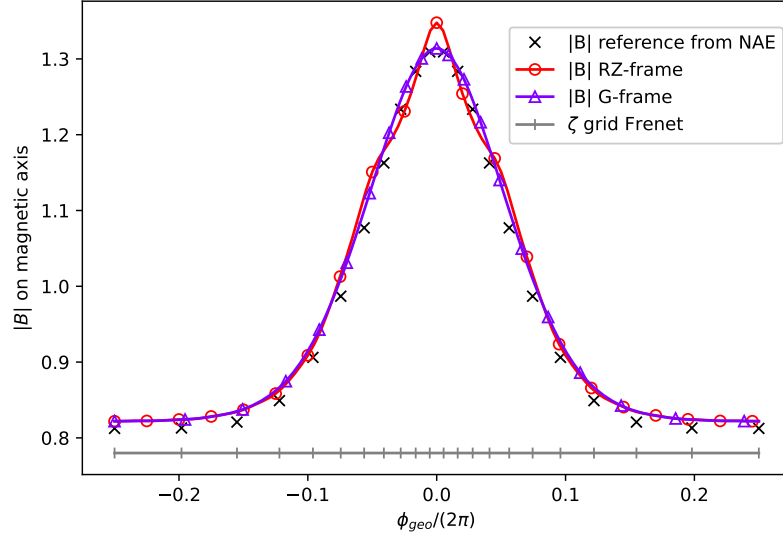


Figure 7. Comparison of the magnetic field strength along the magnetic axis of the equilibrium solutions using the RZ -frame and the G -frame, and the reference solution of the NAE.

From the solution of the NAE, we know the magnetic field strength along the axis, which we will use as a reference. In Fig. 7, we compare to the magnetic field strength along the magnetic axis of the equilibrium solutions with the G -frame and RZ -frame. We chose to plot over the geometric toroidal angle, but also plot the points used for the ‘ ζ -grid’, showing that the parametrization when using the G -frame provides a higher resolution in the region where the magnetic field strength peaks. It is clearly seen that the equilibrium solution with the G -frame is very close to the reference solution, whereas, even with a higher resolution, the equilibrium solution with the RZ -frame struggles to accurately represent the peak. In Fig. 8, cross-sections of the flux surfaces show a clear difference of the equilibrium solution, especially in the strongly shaped cross-sections.

It is expected that the full 3D MHD equilibrium solution using the boundary of the NAE is different from the solution of the NAE. For example, the euclidean distance of the magnetic axis to the axis of the G -frame is on the order of 10^{-4} . But we also know that the 3D MHD equilibrium solution should converge to the solution of the NAE when the boundary is evaluated at a smaller radius. In Fig. 9, we demonstrate the convergence, using GVEC with the G -frame and the same resolution as before, but with the initial average minor radius scaled by a factor of 0.1 and 0.01.

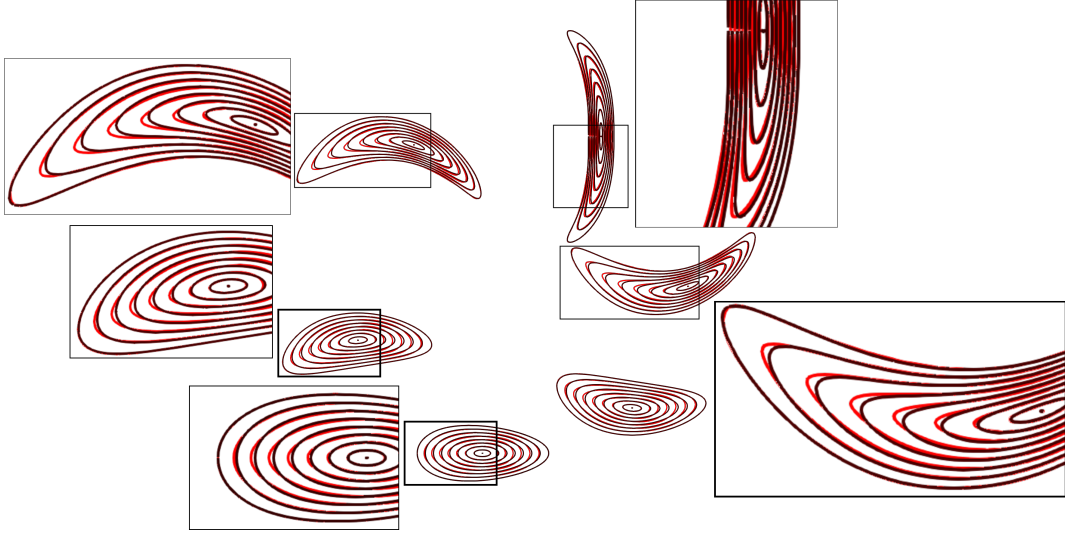


Figure 8. Comparison of the equilibrium solution with the G -frame in black and the RZ -frame in red, showing cross-sections of flux surfaces in (R, Z) -planes over a half field period. The frames show zoomed in views.

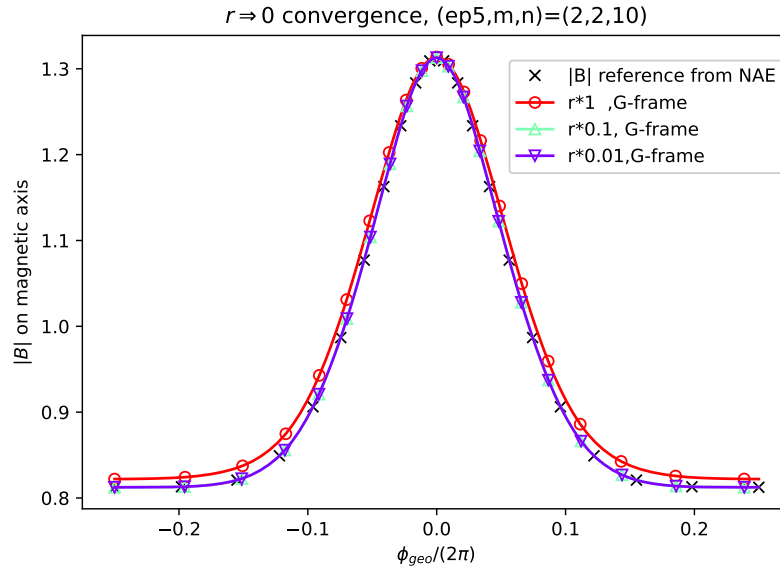


Figure 9. Convergence of the equilibrium solution with the G -frame to the solution of the NAE.

5. Conclusion

In this work, we proposed a new and flexible approach of representing the geometry of 3D MHD equilibria of strongly shaped stellarators. Motivated by the discovery of new configurations found by means of the near-axis expansion (NAE), we adopt the idea of an axis-following frame with cross-sections normal to the axis, instead of the usual cylindrical coordinates (' RZ -frame'). We show the deficiencies of the conventional Frenet frame, such as abrupt sign changes or unnecessary twists and we introduce a

generalized Frenet frame (' G -frame'), which overcomes these deficiencies. We describe the steps needed for implementation of the G -frame in the 3D MHD equilibrium solver GVEC.

Using the G -frame for the particular case of a two-field-periodic QI-configuration, we show that far fewer degrees of freedom are needed for the representation of the boundary, compared to the RZ -frame. Consequently, we found that an accurate equilibrium solution, obtained in GVEC with the G -frame, also needs less resolution and less iterations to converge, compared to the equilibrium solution with the RZ -frame.

Computing 3D MHD equilibria in an RZ -frame has strong limitations on the 3D shapes it can represent, artificially restricting the space of possible shapes in stellarator optimization. We hope that an axis-following frame such as the G -frame will allow the representation of stellarators of any shape with minimal number of degrees of freedom, and thereby open paths for progress in stellarator optimization.

Acknowledgments

The authors would like to thank our colleagues at the Numerical Methods in Plasma Physics division at IPP Garching and the Stellarator Theory group at IPP Greifswald for the insightful discussions and support in this endeavor. We would also like to thank Matt Landreman for a discussion on quasi-helical stellarators that motivated this work.

This work has been carried out within the framework of the EUROfusion Consortium, funded by the European Union via the Euratom Research and Training Programme (Grant Agreement No 101052200 — EUROfusion). Views and opinions expressed are however those of the author(s) only and do not necessarily reflect those of the European Union or the European Commission. Neither the European Union nor the European Commission can be held responsible for them.

Data availability statement

The simulation data presented in this paper is openly available at <https://doi.org/10.5281/zenodo.13960848>.

Appendix A. Second derivatives of the map h with the G -frame

When computing variations of the MHD energy (12) with respect to X^1, X^2 , second derivatives of the map h are needed. Given the map h in (14) using the G -frame, we summarize here the derivatives of the metric terms \mathcal{J}_h and G from (16), with respect to q^1, q^2 . Only first derivatives of X_0, N, B , as already used in (16), will be necessary.

The Jacobian determinant is defined as

$$\begin{aligned}
\mathcal{J}_h^2 &:= \det(G) = G_{11}G_{22}G_{33} + 2G_{12}G_{23}G_{31} - G_{13}^2G_{22} - G_{23}^2G_{11} - G_{12}^2G_{33} \\
&= |N|^2|B|^2|\tilde{T}_q|^2 + 2(N \cdot B)(B \cdot \tilde{T}_q)(N \cdot \tilde{T}_q) - (N \cdot \tilde{T}_q)^2|B|^2 - (B \cdot \tilde{T}_q)^2|N|^2 - (N \cdot B)^2|\tilde{T}_q|^2 \\
&= |N \times B|^2|\tilde{T}_q|^2 + ((N \times B) \cdot (B \times \tilde{T}_q))(N \cdot \tilde{T}_q) + ((B \times N) \cdot (N \times \tilde{T}_q))(B \cdot \tilde{T}_q),
\end{aligned} \tag{A.1}$$

where we used the identity $(a \times b) \cdot (c \times d) = (a \cdot c)(b \cdot d) - (a \cdot d)(b \cdot c)$ holding for any $a, b, c, d \in \mathbb{R}^3$. The derivatives of the Jacobian determinant are conveniently computed from (A.1), with $\frac{\partial \tilde{T}_q}{\partial q^1} = N$ and $\frac{\partial \tilde{T}_q}{\partial q^2} = B$ resulting in

$$\begin{aligned}
\frac{\partial \mathcal{J}_h}{\partial q^1} &= \frac{1}{2\mathcal{J}_h} \frac{\partial \mathcal{J}_h^2}{\partial q^1} = \frac{1}{\mathcal{J}_h} \left[(|N|^2|B|^2 - (N \cdot B)^2) (\tilde{T}_q \cdot N') \right. \\
&\quad + \left((B \cdot N)(B \cdot \tilde{T}_q) - |B|^2(N \cdot \tilde{T}_q) \right) (N \cdot N') \\
&\quad + \left. \left((N \cdot B)(N \cdot \tilde{T}_q) - |N|^2(B \cdot \tilde{T}_q) \right) (B \cdot N') \right] \\
&= \frac{1}{\mathcal{J}_h} \left[|N \times B|^2(\tilde{T}_q \cdot N') \right. \\
&\quad + \left((N \times B) \cdot (B \times \tilde{T}_q) \right) (N \cdot N') \\
&\quad + \left. \left((B \times N) \cdot (N \times \tilde{T}_q) \right) (B \cdot N') \right],
\end{aligned} \tag{A.2}$$

and

$$\begin{aligned}
\frac{\partial \mathcal{J}_h}{\partial q^2} &= \frac{1}{\mathcal{J}_h} \left[|N \times B|^2(\tilde{T}_q \cdot B') \right. \\
&\quad + \left((N \times B) \cdot (B \times \tilde{T}_q) \right) (N \cdot B') \\
&\quad + \left. \left((B \times N) \cdot (N \times \tilde{T}_q) \right) (B \cdot B') \right],
\end{aligned} \tag{A.3}$$

and the derivatives of the metric tensor are

$$\frac{\partial G}{\partial q^1} = \begin{bmatrix} 0 & 0 & N \cdot N' \\ 0 & 0 & B \cdot N' \\ N \cdot N' & B \cdot N' & 2\tilde{T}_q \cdot N' \end{bmatrix}, \quad \frac{\partial G}{\partial q^2} = \begin{bmatrix} 0 & 0 & N \cdot B' \\ 0 & 0 & B \cdot B' \\ N \cdot B' & B \cdot B' & 2\tilde{T}_q \cdot B' \end{bmatrix}. \tag{A.4}$$

All these identities have been directly implemented in GVEC, using the G -frame interface from section 2.1.

References

- [1] Landreman M, Sengupta W and Plunk G G 2019 *Journal of Plasma Physics* **85** 905850103
- [2] Plunk G G, Landreman M and Helander P 2019 *Journal of Plasma Physics* **85** 905850602
- [3] Bishop R L 1975 *The American Mathematical Monthly* **82** 246–251
- [4] Yilmaz S and Turgut M 2010 *Journal of Mathematical Analysis and Applications* **371** 764–776
ISSN 0022-247X
- [5] Wang W, Jüttler B, Zheng D and Liu Y 2008 *ACM Trans. Graph.* **27** ISSN 0730-0301 URL
<https://doi.org/10.1145/1330511.1330513>

- [6] Hirshman S P and Whitson J C 1983 *Physics of Fluids* **26** 3553–3568 ISSN 0031-9171 URL <https://doi.org/10.1063/1.864116>
- [7] Hirshman S, van RIJ W and Merkel P 1986 *Computer Physics Communications* **43** 143–155 ISSN 0010-4655 URL [http://dx.doi.org/10.1016/0010-4655\(86\)90058-5](http://dx.doi.org/10.1016/0010-4655(86)90058-5)
- [8] Hirshman S and Betancourt O 1991 *Journal of Computational Physics* **96** 99–109 ISSN 0021-9991 URL [http://dx.doi.org/10.1016/0021-9991\(91\)90267-0](http://dx.doi.org/10.1016/0021-9991(91)90267-0)
- [9] Huang Y M, Zhou Y, Loizu J, Hudson S and Bhattacharjee A 2023 *Plasma Physics and Controlled Fusion* **65** 129601
- [10] D’haeseleer W D, Hitchon W N G, Callen J D and Shohet J L 1991 *Flux Coordinates and Magnetic Field Structure* (Springer Berlin Heidelberg) ISBN 9783642755958 URL <http://dx.doi.org/10.1007/978-3-642-75595-8>
- [11] Dudt D W and Kolemen E 2020 *Physics of Plasmas* **27** 102513 ISSN 1070-664X URL <https://doi.org/10.1063/5.0020743>
- [12] Hindenlang F, Maj O, Strumberger E, Rampp M and Sonnendrücker E 2019 GVEC: a newly developed 3D ideal MHD Galerkin variational equilibrium code annual Meeting of the Simons Collaboration on Hidden Symmetries and Fusion Energy
- [13] Garren D A and Boozer A H 1991 *Physics of Fluids B* **3** 2805–2821 URL <http://scitation.aip.org/content/aip/journal/pofb/3/10/10.1063/1.859915>
- [14] Garren D A and Boozer A H 1991 *Physics of Fluids B* **3** 2822–2834 URL <http://scitation.aip.org/content/aip/journal/pofb/3/10/10.1063/1.859916>
- [15] Landreman M and Sengupta W 2018 *Journal of Plasma Physics* **84** 905840616
- [16] Landreman M and Sengupta W 2019 *Journal of Plasma Physics* **85** 815850601
- [17] Camacho Mata K, Plunk G G and Jorge R 2022 *Journal of Plasma Physics* **88** 905880503
- [18] Plunk G G *et al.* 2024 A geometric approach to constructing quasi-isodynamic fields *in preparation*
- [19] Tecchiolli Z, Hudson S, Loizu J, Köberl R, Hindenlang F and De Lucca B 2024 *submitted to Journal of Plasma Physics* ArXiv:2405.08173 URL <http://arxiv.org/abs/2405.08173>